Enhanced superconducting properties of double-chain based superconductor $Pr_2Ba_4Cu_7O_{15-\delta}$ synthesized by citrate pyrolysis technique

Kazuma Honnami [a], Michiaki Matsukawa [*,a], Tatsuya Senzaki [a], Tomoki Toyama [a], Haruka Taniguchi [a], Koichi Ui [a], Takahiko Sasaki [b], Kohki Takahashi [b], Makoto Hagiwara [c]

[a] Faculty of Science and Engineering, Iwate University, Morioka 020-8551, Japan
[b] Institute for Materials Research, Tohoku University, Sendai 980-8577, Japan
[c] Kyoto Institute of Technology, Kyoto 606-8585, Japan

ARTICLE INFO

ABSTRACT

We report the enhanced superconducting properties of double-chain based superconductor $Pr_2Ba_4Cu_7O_{15-\delta}$ synthesized by the citrate pyrolysis technique. The reduction heat treatment in vacuum results in the appearance of superconducting state with T_c=22-24 K, accompanied by the higher residual resistivity ratios. The superconducting volume fractions are estimated from the ZFC data to be $50 \sim 55$%, indicating the bulk superconductivity. We evaluate from the magneto-transport data the temperature dependence of the superconducting critical field, to establish the superconducting phase diagram. The upper critical magnetic field is estimated to be about 35 T at low temperatures from the resistive transition data using the Werthamer-Helfand-Hohenberg formula. The Hall coefficient R_H of the 48-h-reduced superconducting sample is determined to be -0.5×10^{-3} cm^3/C at 30 K, suggesting higher electron concentration. These findings have a close relationship with homogeneous distributions of the superconducting grains and improved weak links between their superconducting grains in the present synthesis process.

1. Introduction

Since the discovery of high-T_c copper-oxide superconductors, researches have focused on the unconventional superconductivity on the two-dimensional CuO_2 planes in some cuprates. In quasi one-dimensional (1D) ladder system without CuO_2 planes, it is well known that the superconductivity at T_c= 12 K appears only under the application of high pressure [1]. In a previous study of Pr-based cuprates with metallic CuO double chains and insulating CuO_2 planes, $Pr_2Ba_4Cu_7O_{15-\delta}$ is found to be a new superconductor with a higher T_c (15 K) after a reduction treatment [2]. A nuclear quadrupole resonance (NQR) study has revealed that the newly discovered superconductivity is realized at the CuO double-chain block [3].

Structurally, the Pr-based cuprates, $PrBa_2Cu_3O_{7-\delta}$ (Pr123) and $PrBa_2Cu_4O_8$ (Pr124), are identical to their corresponding Y-based high-T_c superconductors, $YBa_2Cu_3O_{7-\delta}$ (Y123) and $YBa_2Cu_4O_8$ (Y124). Pr123 and Pr124 compounds have insulating CuO_2 planes and are non-superconductive [4,5]. The suppression of superconductivity in the Pr substitutes has been explained by the hybridization of Pr-$4f$ and O-$2p$

orbitals [6]. The crystal structure of Pr124 with CuO double chains differs from that of Pr123 with CuO single chains. It is well known that CuO single chains in Pr123 and CuO double chains in Pr124 show semiconducting and metallic behaviors, respectively [7]. The carrier concentration of doped double chains of Pr124 is difficult to vary, because it is thermally stable up to high temperatures.

The compound $Pr_2Ba_4Cu_7O_{15-\delta}$ (Pr247) is an intermediate between Pr123 and Pr124. In this compound, CuO single-chain and double-chain blocks are alternately stacked along the c-axis such as {-D-S-D-S-} sequence [8,9] (see Fig. 1). Here, S and D denote CuO single-chain and double-chain blocks along the b-axis, respectively. The physical properties of the metallic CuO double chains can be examined by controlling the oxygen content along the semiconducting CuO single chains. Anisotropic resistivity measurements of single-crystal Pr124 have revealed that metallic transport arises by the conduction along the CuO double chains [10]. In oxygen removed polycrystalline $Pr_2Ba_4Cu_7O_{15-\delta}$, the superconductivity appears at an onset temperature $T_{c,on}$ of ∼15 K [2]. Hall coefficient measurements of superconducting Pr247 with $T_{c,on}$ = 15 K have revealed that at intermediate temperatures below 120

ARTICLE IN PRESS

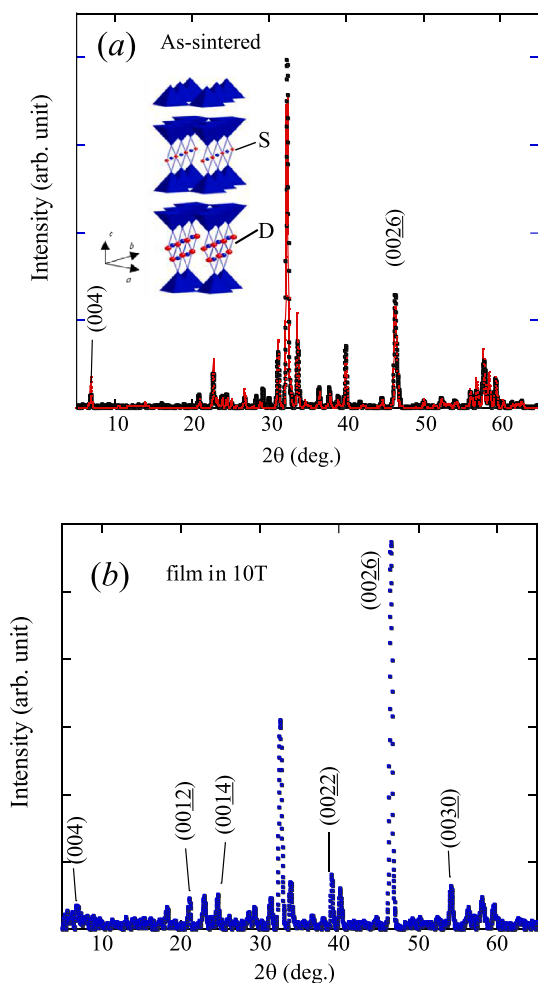K. Honnami et al.   Physica C: Superconductivity and its applications xxx (xxxx) xxx

Fig. 1. (color online)(a) X-ray diffraction patterns of as-sintered polycrystalline $Pr_2Ba_4Cu_7O_{15-\delta}$. The (004) peak corresponds to one of typical Miller indexes of Pr247. The calculated curve is obtained using the lattice parameters in the text. Inset shows the crystal structure of Pr247 with CuO single-chain and double-chain blocks along the b-axis. Here, S and D denote CuO single-chain and double-chain blocks along the b-axis. (b)X-ray diffraction pattern for polycrystalline film prepared by an electrophoretic deposition technique under 10 T. The magnetic field was applied parallel to the direction of applied electric field between anode and cathode electrodes.

K, the main carriers change from holes to electrons, as the temperature decreases. Accordingly, this compound is an electron-doped superconductor [11]. In our previous study, we examined the effect of magnetic fields on the superconducting phase of Pr247 [12]. Despite of the resistive drop associated with the superconducting transition, we found that the diamagnetic signal was strongly suppressed as expected in the 1D superconductivity of CuO double chains. We also reported the effect of pressure on magneto-transport properties in the superconducting and normal phases of the metallic double chain compound $Pr_2Ba_4Cu_7O_{15-\delta}$ [13]. The model of slightly warped Fermi surfaces explains not only the magneto-resistance (MR) effect of the non-superconducting sample, but also the pressure-induced MR phenomena of the superconducting sample.

In this paper, we demonstrate the magneto-transport properties of $Pr_2Ba_4Cu_7O_{15-\delta}$ with $T_{c,on}$ (22–24 K) accompanied by the strongly metallic conduction, for our understanding of the effect of magnetic field on the superconducting properties of electron-doped metallic double-chain compound. In the next section, the experimental outline is described. In Sect. 3, we show the outstanding data including higher residual resistivity ratios, larger superconducting volume fractions,

enhanced zero-resistance states under magnetic field, and higher carrier concentrations. The final section is devoted to the summary.

2. Experiment

Polycrystalline samples of $Pr_2Ba_4Cu_7O_{15-\delta}$ were synthesized by using the citrate pyrolysis technique [14,15]. In the first step, stoichiometric mixtures of high purity Pr_6O_{11}, $Ba(NO_3)_2$, and CuO were dissolved in a nitric acid solution at 50-60 °C. After adding citric acid and neutralizing it by aqueous ammonia, we then obtained the porous products through the self-ignition process using halogen lamp stirrer. In the next step, the precursors were ground and resultant fine powders were annealed under ambient oxygen pressure at 890-891 °C for an extended period over 110-120h. In the present citrate pyrolysis synthesis procedure, we adopted the electric tube furnace with three zone temperature controlled system, to achieve the temperature uniformity within 1 °C.

For scanning electron microscope (SEM) measurements, we prepared the polycrystalline film sample, to reveal microstructures of single-phase $Pr_2Ba_4Cu_7O_{15}$ powders synthesized by the citrate pyrolysis technique. The polycrystalline film on Ag substrate was fabricated from the as-sintered powders by an electrophoretic deposition technique. The electrophoretic deposition was conducted in the acetone and iodine bath under the application of electric voltage up to 300 V for 120 s [16]. We set Pt and Ag plates as anode and cathode electrodes, respectively. Furthermore, we performed the magnetic field assisted electrophoretic deposition process for the fabrication of c-axis aligned $Pr_2Ba_4Cu_7O_{15}$ polycrystalline film [17]. Here, the magnetic anisotropy of rare earth ion Pr including $Pr_2Ba_4Cu_7O_{15}$ shows that the magnetic susceptibility of $\chi_{H\parallel c}$ is larger than that of $\chi_{H\perp c}$ [18]. A magnetic field up to 10 T was applied to the colloid bath including the suspended Pr247 powders using a superconducting magnet with a 100 mm diameter bore at room temperature at the High Field Laboratory for Superconducting Materials, Institute for Materials Research (IMR), Tohoku University. The magnetic field was applied parallel to the direction of applied electric field for the electrophoretic deposition.

We performed X-ray diffraction measurements on the produced samples at room temperature with an Ultima IV diffractometer (Rigaku) using Cu-Kα radiation. The lattice parameters were estimated from the x-ray diffraction data using the least-squares fits.

The oxygen in the as-sintered sample was removed by reduction treatment in a vacuum at 500 °C, yielding a superconducting material. Typical dimensions of the pelletized rectangular sample were $4.2 \times 3.4 \times 1.3$ mm^3. X-ray diffraction data revealed that the as-sintered polycrystalline samples are an almost single phase with an orthorhombic structure ($Ammm$), as shown in Fig. 1(a).

The lattice parameters of the as-sintered sample are $a = 3.89293$ Å, $b = 3.91394$ Å, and $c = 50.79270$ Å, which are in fair agreement with those obtained by a previous study [19]. The oxygen deficiencies in the 48 h and 72 h reduced samples in a vacuum were estimated from gravimetric analysis to be $\delta = 0.43$ and 0.54, respectively. As a function of the oxygen deficiency, the $T_{c,on}$ rises rapidly at $\delta \geq \sim 0.2$, then monotonically increases with increasing δ, and finally saturates around 26-27 K at $\delta \geq \sim 0.6$ [20]. Accordingly, we expect that the carriers in the present sample are concentrated around the optimally doped region.

The electric resistivity in zero magnetic field was measured by the dc four-terminal method. The magneto-transport up to 9 T was measured by the ac four-probe method using a physical property measuring system (PPMS, Quantum Design), increasing the zero-field-cooling (ZFC) temperatures from 4 K to 40 K. The high field resistivity (up to 14 T) was measured in a superconducting magnet at IMR, Tohoku University. The electric current I was applied longitudinally to the sample ; consequently, the applied magnetic field H was transverse to the sample (because $H \perp I$). We performed Hall coefficient measurements on the as-sintered and 48 h reduced samples with the five-probe technique using

PPMS and the 15T-superconducting magnet [21]. The *dc* magnetization was performed under ZFC in a commercial superconducting quantum interference device magnetometer (Quantum Design, MPMS).

3. Results and Discussion

Figure 1 (*a*) shows X-ray diffraction (XRD) patterns of as-sintered polycrystalline $Pr_2Ba_4Cu_7O_{15-\delta}$(Pr247). The (004) peak corresponds to one of typical Miller indexes of Pr247. The calculated curve is obtained using the lattice parameters. The inset of Fig. 1(*a*) displays the crystal structure of Pr247 with CuO single-chain and double-chain blocks along the *b*-axis. The unknown impurity peaks near $2\theta \sim 30°$ are identified as the $BaCuO_2$ phase [15].

For comparison, X-ray diffraction pattern of polycrystalline film prepared by an electrophoretic deposition technique under 10 T is shown in in Fig. 1(*b*). We note that the XRD pattern of the Pr247 film fabricated by the electrophoretic deposition process without the applied magnetic field (not shown here) was the same as that of the Pr247 powders. (00*l*) peaks did not appear except for the (004) and (002̲6̲) peaks. When the magnetic field was applied parallel to the direction of applied electric field, the peak intensities of (00*l*) were strongly enhanced as shown in Fig. 1(*b*), indicating the c-axis alignment of polycrystalline grains. The SEM image of the Pr247 film in Fig. 2 reveals that plate-like grains with sub micron size are homogeneously dispersed.

Now, the temperature dependences of electric resistivities of the as-sintered, 48-h-reduced and 72-h-reduced $Pr_2Ba_4Cu_7O_{15-\delta}$ compounds are shown in Fig. 3(*a*). The reduction heat treatment on the as-sintered sample in vacuum results in the appearance of superconducting state with T_c=22-24 K, accompanied by the strongly metallic properties over a wide range of temperature. Here, we define the residual resistivity ratio (RRR) as $\rho(300K)/\rho(30K)$, For the present samples reduced in vacuum, we obtained the higher RRR values (10 ∼ 12.5), in comparison with the previous data [12].

Furthermore, to check the bulk superconductivity, we performed to measure low-temperature dependences of magnetic susceptibilities χ of the 48-h and 72-h-reduced superconducting samples measured at 5 mT under ZFC scan. Figure 3(*b*) exhibits diamagnetic signals below $T_{c,on}$=22.5 K and 24.0 K for the 48-h-reduced and 72-h-reduced samples, respectively. In addition, the superconducting volume fractions due to the shielding effect are estimated to be 50 ∼ 55% from the ZFC values at 5 K, which are much higher than the previous data (∼ 30%) [12]. In the inset of Fig. 3(*b*), the magnified data are plotted to clarify the definition of $T_{c,on}$. The characteristic values for the present and previous samples are listed in Table 1.

Next, we try to measure the magneto-transport properties of the reduced samples, to examine the magnetic effect on the superconducting phase of the Pr247 compound. Figure 4(*a*) shows the low-temperature
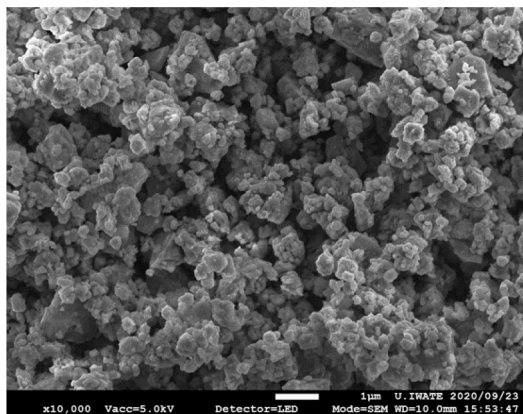

Fig. 2. (color online) SEM image for polycrystalline film prepared by an electrophoretic deposition technique under 10 T.
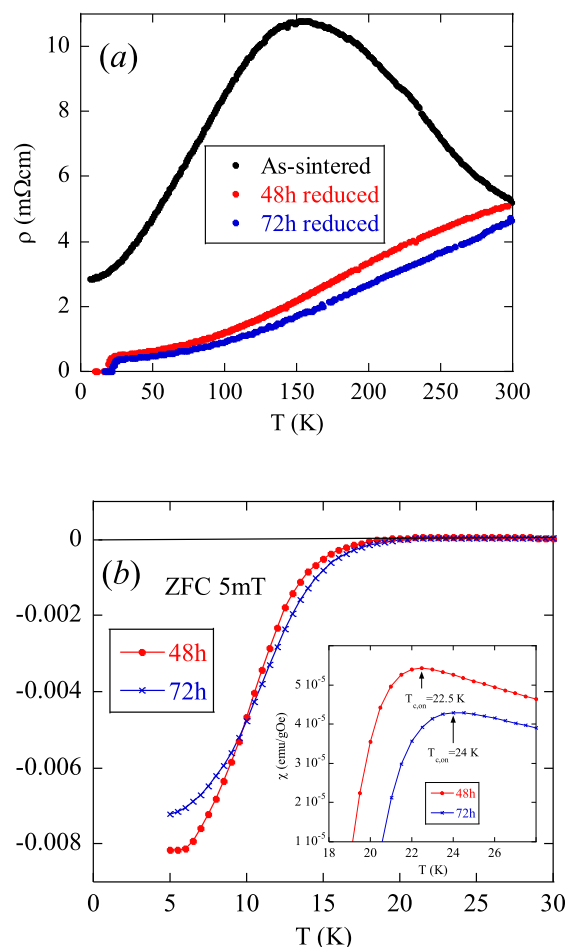

Fig. 3. (color online)(a) Temperature dependences of electric resistivities of the as-sintered, 48-h-reduced and 72-h-reduced $Pr_2Ba_4Cu_7O_{15-\delta}$ compounds. (b) low-temperature dependences of magnetic susceptibilities χ of the 48-h-reduced and 72-h-reduced superconducting samples measured at 5 mT under ZFC scan. In the inset, the magnified data are plotted to clarify the definition of $T_{c,on}$.

dependences of electric resistivities of the 48-h-reduced superconducting $Pr_2Ba_4Cu_7O_{15-\delta}$ compound measured under zero field and applied fields of 10 and 14T.

In zero field, the resistivity starts to decrease around $T_{c,on}$ = 22 K, then follows a rapid drop, and finally achieves a zero-resistance state at $T_{c,zero}$ = ∼18 K. The observed transition width $T_{c,on}$ = 22 K is relatively sharp in comparison with the published data. Inset plots the magneto-resistance data of the 48-h-reduced sample at 4.2 and 30 K. At the high field of 10 T, we observed $T_{c,on}$ = 18 K and $T_{c,zero}$ = ∼5 K. Upon increasing the applied field up to 14 T, the superconductive critical field at 4.2K is determined to be 10.6 T. Even at the maximum field of 14 T, we judge that the zero-resistance state is almost realized over the whole sample since the magnitudes of ρ are negligibly small with those of the normal state at 30 K. These findings strongly suggest that for the present sample the superconducting properties under relatively high fields are considerably improved. For the previous Pr247 samples, it has been reported that the critical field is as low as a few tesla at low temperatures.

In Fig. 4(*b*), we show the low-temperature dependences of electric resistivities of the 72-h-reduced superconducting $Pr_2Ba_4Cu_7O_{15-\delta}$ compound measured at the several applied fields ($H = 0, 1, 3, 6$ and 9 T). The inset displays the enlarged data of the 72-h-reduced sample around $T_{c,on}$ = 24.3 K. In a similar to the data of the 48-h-reduced sample, we observed a zero-resistance state below $T_{c,zero}$ = ∼18 K and 5 K, at 0 T and at 9 T, respectively. Here, we evaluate from the magneto-transport data

ARTICLE IN PRESS

K. Honnami et al.   Physica C: Superconductivity and its applications xxx (xxxx) xxx

Table 1

Physical and superconducting properties for $Pr_2Ba_4Cu_7O_{15-\delta}$. In details, see the corresponding text and references. δ and RRR denote oxygen deficiency and residual resistivity ratio $\rho(300K)/\rho(30K)$, respectively. f_{SC}: the superconducting volume fraction estimated from the ZFC magnetization data at low temperatures. H_c^* is defined from the field sweep data at fixed temperatures as the critical field where the zero-resistance state is violated with increasing the field.

Synthesis	Reduced time	δ	RRR	f_{SC} (%)	$T_{c,on}$ (K)	$T_{c,zero}$ (K)	H_c^* (T)	$R_H(30K)$ (10^{-3} cm³/C)
citrate pyrolysis	48h	0.43	10	55	22	18	10.6(4.2K)	-0.5
citrate pyrolysis	72h	0.54	12	50	24.3	18	-	-
citrate pyrolysis	48h	0.52[a]	4[a]	30[a]	26.5[a]	15[a]	~2(5K)	-1.1[b]
sol-gel [22]	72h	0.94	2	~10	30.5	~10	-	-
high pressure [11]	48h	0.5	-	30	16	~10	-	-1.5

[a] see ref. [12]
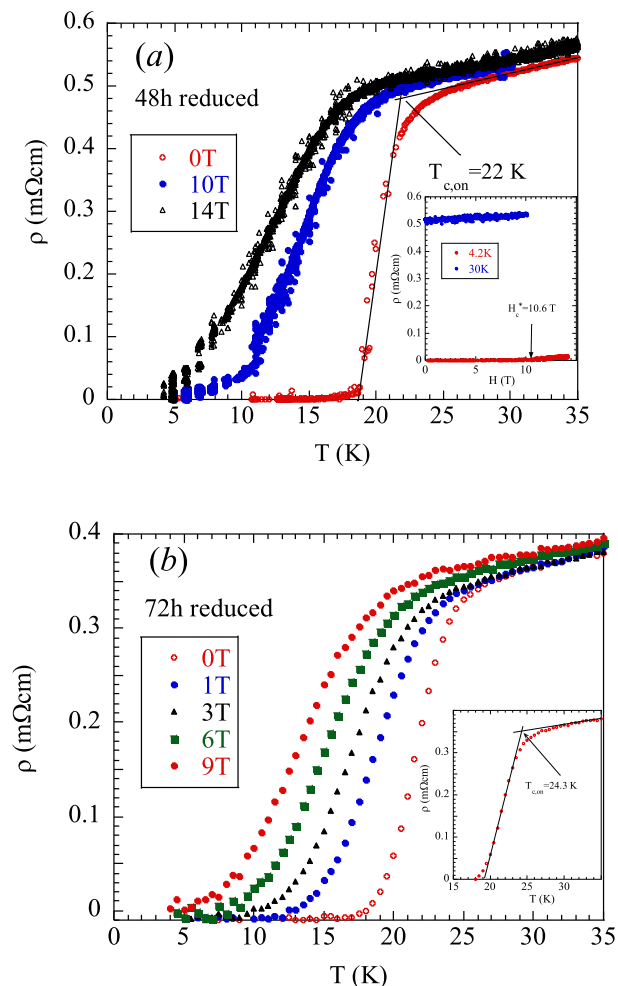[b] ref. [21]

Fig. 4. (color online) (a) Low-temperature dependences of electric resistivities of the 48-h-reduced superconducting $Pr_2Ba_4Cu_7O_{15-\delta}$ compound measured under 0T, 10T, and 14T. Inset plots the magneto-resistance data of the 48-h-reduced sample at 4.2 K and 30 K. (b) Low-temperature dependences of electric resistivities of the 72-h-reduced superconducting $Pr_2Ba_4Cu_7O_{15-\delta}$ compound measured at the several applied fields ($H = 0, 1, 3, 6$ and 9 T). The inset displays the enlarged data of the 72-h-reduced sample around T_c.

the temperature dependence of the superconductive critical field, to establish the superconducting phase diagram. The onset T_c ($T_{c,on}$) is determined from the intersection between the two lines extrapolated from the normal and superconducting transition resistivity data, just above and bellow T_c, respectively. (see Fig. 4). The zero-point T_c ($T_{c,zero}$) denotes the value of the critical temperature reaching the zero-

resistance state. The upper critical field at 0 K is estimated to be about 35 T from the data of the onset T_c using the Werthamer-Helfand-Hohenberg (WHH) formula in the dirty limit, $\mu_0 H_{c2}(0) = -0.69 T_c (dH_{c2}(T)/dT)|_{T=T_c}$ [23].

There are quite differences in the critical fields determined from $T_{c,zero}$ between the present and previous samples, strongly suggesting the enhanced superconducting properties in the presence of magnetic field as represented by a right arrow in Fig. 5.

Furthermore, in Fig. 6, we show the temperature dependences of the Hall coefficients R_H for the as-sintered non-superconducting and 48-h-reduced superconducting samples of $Pr_2Ba_4Cu_7O_{15-\delta}$. The R_H data of the as-sintered sample are very similar, in the both magnitude and temperature dependence, to those of the previous sample. For the 48-h-reduced sample, the R_H data exhibit negative values in the limited temperature range between 30 and 80 K, accompanied by electron doping due to the reduced heat treatment in vacuum. Moreover, we estimate $R_H = -0.5 \times 10^{-3}$ cm³/C at 30 K, which is as about half as the published data [21], indicating higher carrier concentration. These results have a close relationship with the enhanced superconducting properties, leading to the superconducting phase diagram of the present samples.

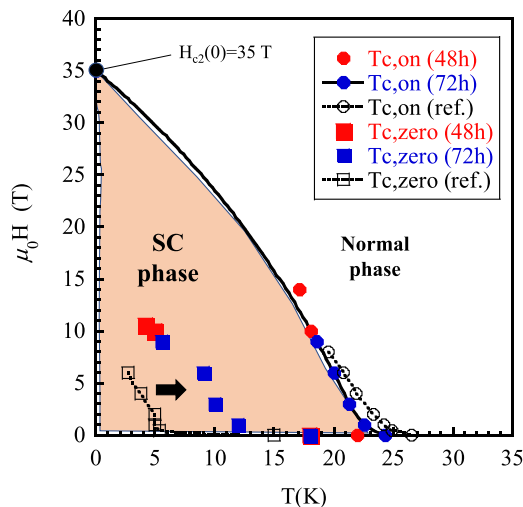Finally, the physical and superconducting properties for $Pr_2Ba_4Cu_7O_{15-\delta}$ compounds are summarized in Table 1. In the present

Fig. 5. (color online) Temperature dependence of the superconducting (SC) critical field of the reduced samples of $Pr_2Ba_4Cu_7O_{15-\delta}$. The onset T_c ($T_{c,on}$) is determined from the resistivity data as described in the text. For comparison, the previous data of the reduced Pr247 are referred (open symbol). The solid curve separating the superconducting and normal phases was the best fit to the experimental data and the upper critical field of ~35 T. Here, the corresponding $H_{c2}(0)$ is estimated using the WHH formula in the text.
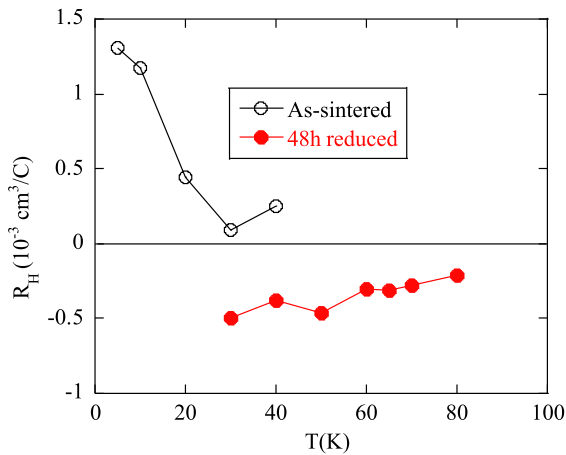
Fig. 6. (color online) Temperature dependences of the Hall coefficients R_H for the as-sintered non-superconducting and 48-h-reduced superconducting samples of $Pr_2Ba_4Cu_7O_{15-\delta}$.

citate pyrolysis synthesis procedure, we adopted the electric tube furnace with three zone temperature controlled system, to achieve the temperature uniformity within 1 K. In spite of limited heat-treatment conditions, we obtained homogeneous distributions of the superconducting grains and improved weak links between their superconducting grains, leading to the enhanced superconducting properties in the present samples. The former is closely related to the narrower transition width of superconductivity in zero magnetic field. The latter improvement is mainly responsible for the considerable enhancement of superconducting properties in high field. In addition, we give some comments on the high-T_c samples synthesized by a sol-gel technique [22]. The transmission electron microscopy image of the high-T_c sample with $T_{c,on}$ =30.5 K revealed that there exists an irregular long-period stacking structure along the c-axis such as {-D-D-D-S-S-S-D-D-S-S} sequences [12]. Here, S and D denote CuO single-chain and double-chain blocks along the b-axis. This finding is close to higher concentration, resulting in higher T_c, in comparison to the regular stacking case of {-S-D-S-D-S-D}. The sol-gel sample showed highly inhomogeneous features such as the irregular stacking structures and the coexistence of the nominal Pr247 phase with the Pr123 and Pr124 phases. For the corresponding inhomogeneous sample, we also observed a broad width between the onset and zero transition temperatures as listed in Table 1.

4. Summary

We have demonstrated the enhanced superconducting properties of double-chain based superconductor $Pr_2Ba_4Cu_7O_{15-\delta}$ synthesized by the citrate pyrolysis technique using the 3-zone controlled electric furnace. The outstanding experimental data include the higher residual resistivity ratios, the larger superconducting volume fractions, the enhanced zero-resistance state under magnetic field, and the higher carrier concentrations.

The SEM image of the Pr247 film revealed that plate-like grains with sub micron size are homogeneously dispersed. For the polycrystalline bulk samples, we obtained the higher residual resistivity ratio ranging from 10 to 12 for the 48-72 h reduction. The reduction heat treatment on the as-sintered sample in vacuum results in the appearance of superconducting state with T_c=22-24 K, accompanied by the metallic properties over a wide range of temperature. The superconducting volume fractions are estimated from the ZFC data to be 50 $\sim$ 55%, indicating the bulk superconductivity. We evaluated from the magneto-transport data the temperature dependence of the superconductive critical field, to

establish the superconducting phase diagram. The upper critical magnetic field was estimated to be about 35 T from the resistive transition data using the WHH formula. For the 48-h-reduced sample, the R_H data exhibit negative values in the limited temperature range between 30 and 80 K, accompanied by electron doping due to the reduced heat treatment in vacuum. Moreover, we estimated $R_H = -0.5 \times 10^{-3}$ cm^3/C at 30 K, which is as about half as the published data, indicative of higher carrier concentration. In spite of limited heat-treatment conditions for the Pr247 phase, we attained homogeneous distributions of the superconducting grains and improved weak links between their superconducting grains, leading to the enhanced superconducting properties in the present samples.

Declaration of Competing Interest

The authors declare that they have no known competing financial interests or personal relationships that could have appeared to influence the work reported in this paper.

Acknowledgement

References

[1] M. Uehara, T. Nagata, J. Akimitsu, H. Takahashi, N. Mori, K. Kinoshita, J. Phys. Soc. Jpn. 65 (1996) 2764.
[2] M. Matsukawa, Y. Yamada, M. Chiba, H. Ogasawara, T. Shibata, A. Matsushita, Y. Takano, Physica C 411 (2004) 101.
[3] S. Watanabe, Y. Yamada, S. Sasaki, Physica C 426-431 (2005) 473.
[4] L. Soderholm, K. Zhang, D.G. Hinks, M.A. Beno, J.D. Jorgensen, C.U. Segre, I. K. Schuller, Nature 328 (1987) 604.
[5] S. Horii, Y. Yamada, H. Ikuta, N. Yamada, Y. Kodama, S. Katano, Y. Funahashi, S. Morii, A. Matsushita, T. Matsumoto, I. Hirabayashi, U. Mizutani, Physica C 302 (1998) 10.
[6] R. Fehrenbacher, T.M. Rice, Phys. Rev. Lett. 70 (1993) 3471.
[7] T. Mizokawa, C. Kim, Z.-X. Shen, A. Ino, T. Yoshida, A. Fujimori, M. Goto, H. Eisaki, S. Uchida, M. Tagami, K. Yoshida, A.I. Rykov, Y. Siohara, K. Tomimoto, S. Tajima, Y. Yamada, S. Horii, N. Yamada, Y. Yamada, I. Hirabayashi, Phys. Rev. Lett. 85 (2000) 4779.
[8] P. Bordet, C. Chaillout, J. Chenavas, J.L. Hodeau, M. Marezio, J. Karpinski, E. Kaldis, Nature 334 (1988) 596.
[9] Y. Yamada, S. Horii, N. Yamada, Z. Guo, Y. Kodama, K. Kawamoto, U. Mizutani, I. Hirabayashi, Physica C 231 (1994) 131.
[10] S. Horii, U. Mizutani, H. Ikuta, Y. Yamada, J.H. Ye, A. Matsushita, N.E. Hussey, H. Takagi, I. Hirabayashi, Phys. Rev. B 61 (2000) 6327.
[11] A. Matsushita, K. Fukuda, Y. Yamada, F. Ishikawa, S. Sekiya, M. Hedo, T. Naka, Science and Technology of Advanced Materials 8 (2007) 477.
[12] T. Chiba, M. Matsukawa, J. Tada, S. Kobayashi, M. Hagiwara, T. Miyazaki, K. Sano, Y. Ono, T. Sasaki, J. Echigoya, J. Phys. Soc. Jpn. 82 (2013) 074706.
[13] M. Kuwabara, M. Matsukawa, K. Sugawara, H. Taniguchi, A. Matsushita, M. Hagiwara, K. Sano, Y. Ono, T. Sasaki, J. Phys. Soc. Jpn. 85 (2016) 124704.
[14] K. Koyama, A. Junod, T. Graf, G. Triscone, J. Muller, Physica C 185-189 (1991) 66.
[15] M. Hagiwara, T. Shima, T. Sugano, K. Koyama, M. Matsuura, Physica C 445-448 (2006) 111.
[16] M. Kawachi, N. Sato, E. Suzuki, S. Ogawa, K. Noto, M. Yoshizawa, Physica C 357-360 (2001) 1023.
[17] M. Kawachi, N. Sato, K. Noto, M. Yoshizawa, Physica C 802-805 (2002) 802.
[18] X. Xu, A. Carrington, A.I. Coldea, A. Enayati-Rad, A. Narduzzo, S. Horii, N. E. Hussey, Phys. Rev. B 81 (2010) 224435.
[19] Y. Yamada, A. Matsushita, Physica C 426-431 (2005) 213.
[20] M. Hagiwara, S. Tanaka, T. Shima, K. Gotoh, S. Kanda, T. Saito, K. Koyama, Physica C 468 (2008) 1217.
[21] J. Tada, M. Matsukawa, T. Konno, S. Kobayashi, M. Hagiwara, T. Miyazaki, K. Sano, Y. Ono, A. Matsushita, J. Phys. Soc. Jpn. 82 (2013) 105003.
[22] S. Toshima, M. Matsukawa, T. Chiba, S. Kobayashi, S. Nimori, M. Hagiwara, Physica C 480 (2012) 1.
[23] N.R. Werthamer, E. Helfand, P.C. Hohenberg, Phys. Rev. 147 (1966) 295.